A New Algorithm for the Quantitation of Myocardial Perfusion SPECT. I: Technical Principles and Reproducibility

Guido Germano, Paul B. Kavanagh, Parker Waechter, Joseph Areeda, Serge Van Kriekinge, Tali Sharir, Howard C. Lewin, and Daniel S. Berman

Departments of Medicine and Imaging, Cedars-Sinai Research Institute, Cedars-Sinai Medical Center, Los Angeles; Departments of Radiological Sciences and Medicine, School of Medicine, University of California, Los Angeles, California

We have developed a new, completely automatic 3-dimensional software approach to quantitative perfusion SPECT. The main features of the software are myocardial sampling based on an ellipsoid model; use of the entire count profile between the endocardial and epicardial surfaces; independence of the algorithm from myocardial shape, size, and orientation and establishment of a standard 3-dimensional point-to-point correspondence among all sampled myocardial regions; automatic generation of quantitative measurements and 5-point semiquantitative scores for each of 20 myocardial segments and automatic derivation of summed perfusion scores; and automatic generation of normal limits for any given patient population on the basis of data fractionally normalized to minimize hot spot artifacts. **Methods:** The new algorithm was tested on the tomographic images of 420 patients studied with a rest ^{201}Tl (111–167 MBq, 35 s/projection)–stress ^{99m}Tc-sestamibi (925–1480 MBq, 25 s/projection) separate dual-isotope protocol on a single-detector camera, a dual-detector 90° camera, and a triple-detector camera. **Results:** The algorithm was successful in 397 of 420 patients (94.5%) and 816 of 840 image datasets (97.1%), with a statistically significant difference between the success rates of the ^{201}Tl images (399/420, or 95.0%) and the ^{99m}Tc images (417/420, or 99.3%; $P <$ 0.001). Algorithm failure was caused by extracardiac uptake (10/24, or 41.7%) or inaccurate identification of the valve plane because of low count statistics (14/24, or 58.3%) and was obviated by simply limiting the image volume in which the software operates. Reproducibility of measurements of summed perfusion scores ($r = 0.999$ and 1 for stress and rest, respectively), global defect extent ($r = 0.999$ and 1 for stress and rest, respectively), and segmental perfusion scores (exact agreement = 99.9%, $\kappa = 0.998$ for stress and 0.997 for rest) was extremely high. **Conclusion:** Automatic 3-dimensional quantitation of perfusion from ^{201}Tl and ^{99m}Tc-sestamibi images is feasible and reproducible. The described software, because it is based on the same sampling scheme used for gated SPECT analysis, ensures intrinsically perfect registration of quantitative perfusion with quantitative regional wall motion and thickening information, if gated SPECT is used.
Key Words: myocardial perfusion SPECT; dual isotope; automatic quantitation; expert systems
J Nucl Med 2000; 41:712–719

Techniques for the quantitation of myocardial perfusion from planar and tomographic images have been developed and refined over the past 2 decades, and the quantitative approach is generally recognized as a desirable tool to standardize analysis and improve the reproducibility of nuclear cardiac assessment (*1–15*). The traditional way of quantitating perfusion involves extraction of a maximal-count circumferential profile from each short-axis image in the stress and rest data sets, according to a hybrid sampling scheme that models the left ventricular myocardium as cylindric in its most basal two thirds and spheric at the apex (*16*). The circumferential profiles (each comprising 36–60 equally spaced maximal-count samples) constitute a condensed or parametric representation of myocardial perfusion and can be combined in 2-dimensional polar, or bull's-eye, maps (*10*). A polar map consists of circumferential profiles (proportional in number to the number of short-axis slices, i.e., to the size of the myocardium) displayed as concentric annuli or rings having either the same thickness (distance-weighted maps) or thicknesses representative of the volume of the myocardium in the individual slices (volume-weighted maps) (*17*). Polar maps from healthy individuals or patients with a low likelihood of coronary artery disease are pooled, and a fixed number of normal circumferential profiles (12 in the hybrid cylindric–spheric approach) are taken to represent the average radioactivity uptake (radioisotope- and gender-specific) in a healthy individual's myocardium (*13,18*). Criteria are established for abnormality of a specific region of the myocardium, and limits of normality are derived from the mean and SD of normal uptake in that region. As a result, the circumferential profiles for every patient can be matched to these normal limits, and the extent to which uptake falls below them can be measured regionally and globally.

This slice-based approach to perfusion quantitation was practical in the days when nuclear medicine computers were slow and proprietary—constraints we have since overcome. Moreover, the growing acceptance of gated SPECT and related function quantitation has stressed the limitations of

slice-based analysis, because the myocardium moves across the slice planes during the cardiac cycle. As a result, the trend has been toward truly 3-dimensional sampling, analysis, and quantitation of the myocardium, particularly in conjunction with the integrated assessment of myocardial perfusion and function (19–21). Here, we describe a 3-dimensional perfusion quantitation algorithm based on our previously described quantitative gated SPECT algorithm for the measurement of global and regional function, and we examine its success rate and the reproducibility of its quantitative measurements in a large number of patients (21,22). The 2 algorithms can easily be integrated to yield automatic and intrinsically registered measurements of perfusion and function from gated myocardial perfusion SPECT data sets (23).

MATERIALS AND METHODS

Segmentation

The quantitative perfusion SPECT (QPS) algorithm starts by segmenting the left ventricle, as previously described (21). In brief, the maximal-count value in the upper half of the ungated 64 × 64 × length (length < 64) short-axis image volume was initially assumed to be part of the myocardium. The threshold of the entire image volume was then set at 50% of the maximal-count value, the image was put in binary form, and the binary clusters (sets of connected voxels) in the volume were determined. All clusters physiologically too small (<50 mL) to represent the left ventricular myocardium were eliminated. For each remaining cluster, the smallest rectangle that circumscribed the left ventricular myocardium in every short-axis slice was determined. If only 1 cluster remained and its bounding rectangle had an aspect ratio close to 1, it was taken to correctly identify the left ventricular myocardium. If 2 or more clusters remained, the cluster closest to the center of the upper right quadrant of the short-axis image volume was chosen. In either case, if the bounding rectangle of the cluster was physiologically too large (>1000 mL) or had an aspect ratio much different from 1, the cluster was iteratively eroded until it broke into 2 or more pieces, and iterative dilation of the 2 largest clusters was performed until the original threshold for the maximal-count value divided by 2 was reached. The binary cluster representing the left ventricle was chosen on the basis of the expected size and location

of the left ventricle and was used as a 3-dimensional mask in the subsequent phase of the algorithm.

Sampling

The center of mass (COM) of the 3-dimensional binary mask segmenting the left ventricular myocardium was located within the left ventricular cavity even in the presence of large perfusion defects, if segmentation of the left ventricle was successful. Radial count profiles originating from the COM were generated to obtain an initial spheric sampling of the product of the binary mask and the short-axis image volume. Sampling occurred every 10° longitudinally (18 total) and every 10° latitudinally (36 total), resulting in 684 count profiles. The locus of the first maxima identified the maximal-count myocardial surface, which was an acceptable proxy for the midmyocardial surface, and was fitted to an ellipsoid as previously reported (24). The fitting process was then iteratively repeated using a new origin for the sampling coordinate system, determined as the projection of the original COM onto the long axis of the ellipsoid. The resulting ellipsoid provided a basis for sampling, in that count profiles normal to the ellipsoid (24 latitudinally, 32 longitudinally, 768 total) were extracted. As shown in Figure 1, this approach would be expected to be more consistent with the actual shape of the myocardium than is the conventional hybrid cylindric–spheric sampling scheme, in which the basal two thirds of the myocardium are modeled as cylindric and the apex is modeled as hemispheric (13,16). The sampling grid from which the ellipsoid normal values subtend was defined as the intersections of the 24 latitudes coplanar with, and the 32 longitudes perpendicular to, its long axis.

Extraction of Perfusion Information

All count profiles normal to the midmyocardial surface were truncated at a distance of 20 mm in both directions from that surface. An asymmetric gaussian curve was then fitted to each profile, and the inner (SD_{in}) and outer (SD_{out}) SDs of the gaussian distribution were noted. The SDs measured from count profiles with peaks falling below 50% of the maximal myocardial count were labeled as invalid and replaced with SDs that minimize the sum of the absolute differences between each invalid SD and the SD of each of its 4 spatial neighbors. For each profile, endocardial and epicardial surface points were defined as points lying an optimal percentage of SD_{in} inward and an optimal percentage of SD_{out} outward, respectively, from the midmyocardial surface along its perpendicular as validated by a cardiac phantom as previously
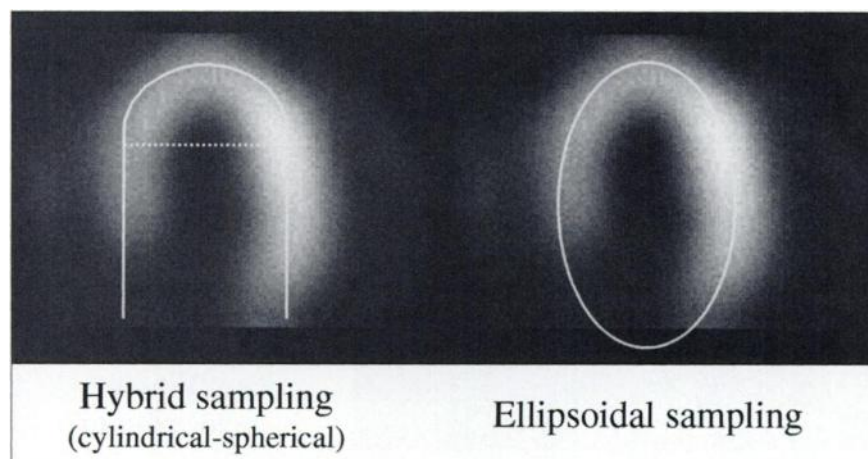

FIGURE 1. Comparison of conventional hybrid (cylindric–spheric) sampling and ellipsoid sampling. In both cases, sampling rays are drawn perpendicularly to geometric surfaces.

described (*21*). Midmyocardial surface points were generated even for severely underperfused areas using myocardial likelihood profiles, a result of the convolution of count profiles extracted with a feature detector, the double derivative of a gaussian distribution with an SD of 10 mm, from unmasked images without thresholds (*21*).

Unlike previous perfusion quantitation approaches based on maximal-count sampling, which uses the maximal pixel count along each sampling profile, our algorithm was based on the average of all perfusion data points comprised between the endocardial and the epicardial surface along count profiles (whole-myocardium sampling, Fig. 2) (*13,16*). In practice, at least 2–3 voxels were averaged for standard zoom–matrix combinations and normal myocardia (more for particular types of patients). Better noise characteristics for the sampled perfusion data, compared with the maximal-count approach, would be the expected result. Moreover, our algorithm was not based on circumferential profiles, in the sense that it did not generate several profiles equal to the number of myocardial short-axis slices for a particular patient. Rather, every myocardium was sampled 3-dimensionally according to the ellipsoid model, and a standard number of equidistant data samples was extracted regardless of myocardial size. With this approach, homologous points in different myocardia were intrinsically registered and could be pooled for generation of normal limits. Also, each point was weighted by the area of the surface patch to which it corresponded, to reflect the curvature of the specific myocardium analyzed at different sampling locations.

Display of Perfusion Information

The perfusion data extracted can be displayed 2-dimensionally or 3-dimensionally, as shown in Figure 3. These representations are parametric, in that only a portion of the information contained in the original image data volume is displayed. Parametric displays based on whole-myocardium sampling theoretically contain more information than do traditional, maximal-count polar map displays, because each sampling point pools perfusion information from multiple image voxels.

Computer-Guided Visual Scoring

The method of visual myocardial perfusion scoring used by Cedars-Sinai Medical Center (CS-20) is based on a 20-segment, 5-point model comprising 6 segments in each of 3 short-axis slices (distal [apical], mid, and basal), the apex being represented by 2 segments visualized in a midvertical long-axis image (Fig. 4). Figure 4 exemplifies only the process, because visual scoring must assess every short-axis slice reconstructed. Our algorithm facilitates visual scoring of myocardial perfusion. Because the endocardial and epicardial surfaces were automatically determined, visual scoring could be guided by software-generated, color-coded segmental boundaries laid over the interleaved stress–rest short-axis images (Fig. 5). The summed stress score (SSS) and summed rest score (SRS) were defined as the sum of the 20 segmental stress and rest scores, respectively (*25,26*).

Generation of Normal Limits

Generation of normal limits was automatic and started with the calculation of normal pixel count values (mean ± SD of homologous pixel count values from the parametric images of several patients with a low likelihood of coronary artery disease). Each parametric image was normalized to 90% of its maximal count so as to reduce the effect of hot spot artifacts. The criteria for perfusion abnormality for each of the 20 myocardial segments were determined by applying automatic receiver operating characteristic analysis to the comparison of quantitative algorithm values and visual scores using a group of patients with appropriately represented segmental perfusion defects (development group). In practice, the quantitative threshold value for segmental abnormality was defined (on a segment-by-segment basis) as the number of SDs below the mean uptake value of that segment in the low-likelihood group that yields optimal sensitivity and specificity for the visual detection of abnormality (score ≥ 2) in the segment. The user interface of the algorithm allows building of the low-likelihood and development-group databases (*13,14*). The remainder of the process, involving the iterative evaluation of multiple (>100) SDs for each segment and the generation of optimal normal limits, was automatic. The development and validation of normal limits for a separate dual-isotope rest ^{201}Tl–stress ^{99m}Tc-sestamibi protocol using this algorithm has been described (*27*).

Extent and Severity of Perfusion Defects

The algorithm offers several ways to express the quantitative extent of perfusion defects. The percentage of abnormal myocar-

FIGURE 2. Comparison of conventional maximal-count and whole-myocardium extraction of myocardial uptake information for analysis and parametric display. Latter uses all points between algorithm-determined endocardial and epicardial boundaries.
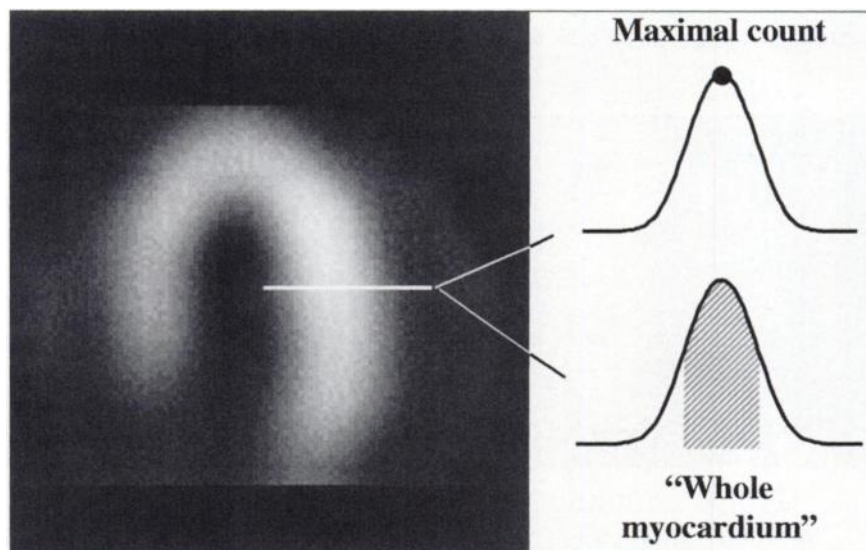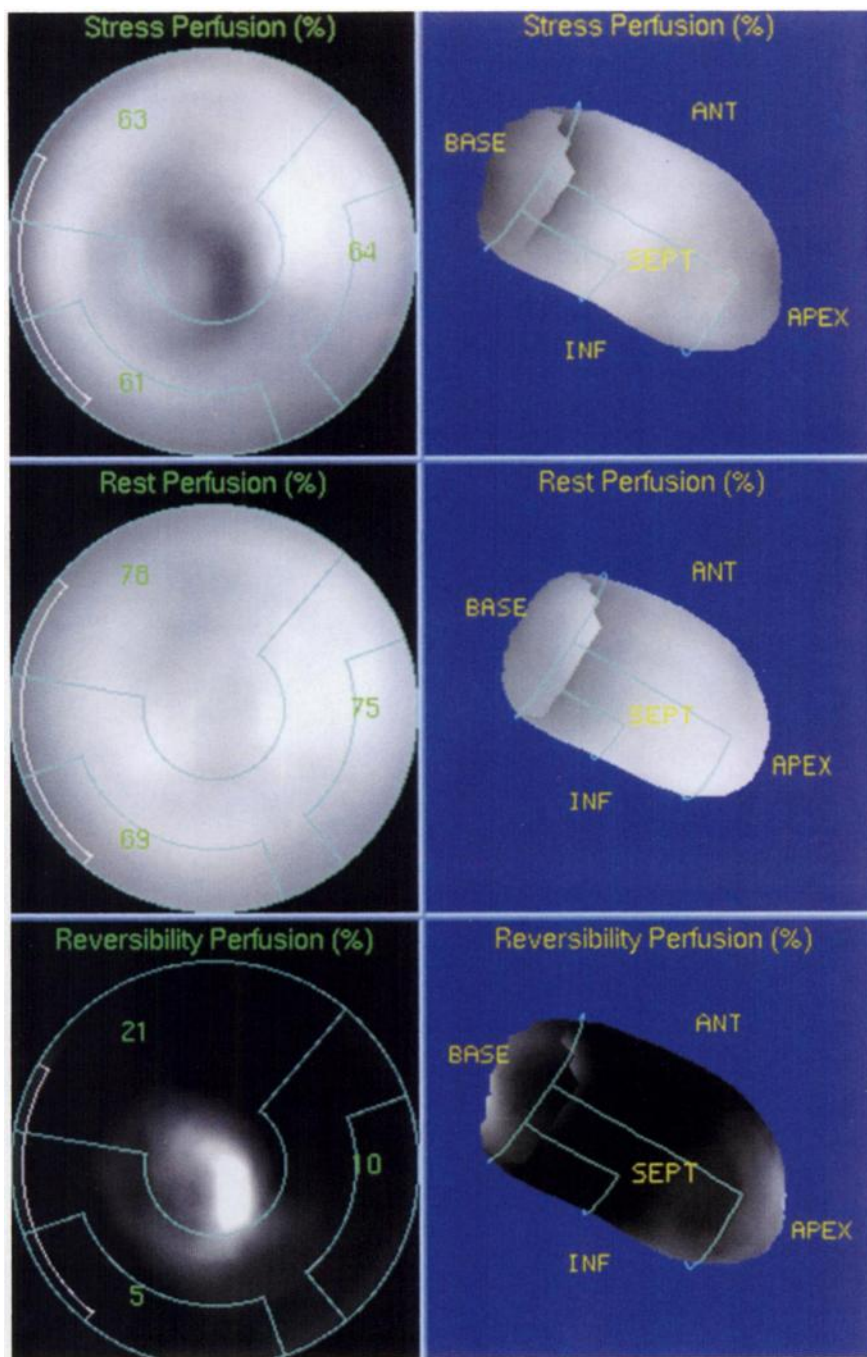
FIGURE 3. Distance-weighted 2-dimensional polar maps (left) and 3-dimensional displays (right) for stress (top), rest (middle), and difference or reversible myocardial uptake (bottom). Standard coronary artery territories are superimposed on all images.

dial pixels in each segment, vascular territory, or wall can be displayed over a standard 2-dimensional parametric blackout map (Fig. 6, top row). Also, the global percentage of abnormal myocardial pixels can be expressed as a numeric value (9). Finally, an estimation of the global quantitative extent of perfusion defects can be derived by multiplying the number of abnormal segments by 5% (in the 20-segment model), this notation being applicable to quantitative and visual scoring alike. Quantitative perfusion defect severity was calculated by multiplying each abnormal pixel by the number of SDs by which its counts fell below normal (13), then grouping the results regionally (Fig. 6, bottom row) or globally, as for defect extent.

Automatic Computer Scoring

The algorithm was also capable of generating semiquantitative 20-segment scores (5-point scale) analogous to those used in visual assessment of perfusion. In practice, normalized count thresholds were iteratively determined for each segment and each semiquantitative category (0 through 4). When used to convert absolute quantities to categoric quantities, these thresholds maximize the agreement between the categorized quantitative measurements and the visual scores in an appropriate patient population, as measured by the value of κ for the relative 5×5 agreement table. Once determined for a given radiopharmaceutical or protocol, the same thresholds can be applied to any patient study acquired under the

FIGURE 4. Twenty-segment, 5-point model used for semiquantitative visual scoring of perfusion.
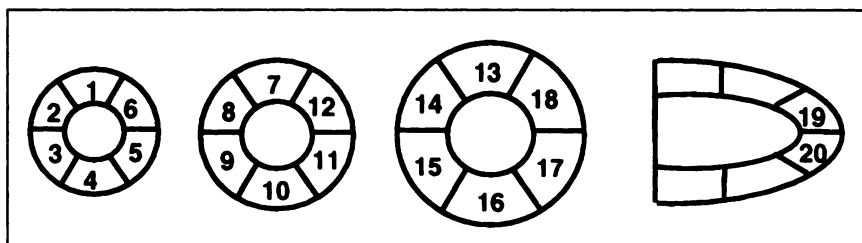
same conditions. As with visual scores, summed stress and rest scores can be derived for the automatic segmental scores.

Patient Studies

The success of the perfusion quantitation algorithm (ability to correctly identify the endocardial and epicardial surfaces of the left ventricle and the valve plane, as visually judged by an expert observer) was tested on 420 clinical patients undergoing a rest [201]Tl (111–167 MBq)–stress ^{99m}Tc-sestamibi (925–1480 MBq) separate-acquisition dual-isotope SPECT protocol (28). The studies were performed using a 2-detector 90° camera (Vertex; ADAC Laboratories, Milpitas, CA), a 3-detector camera (Prism; Picker Interna-
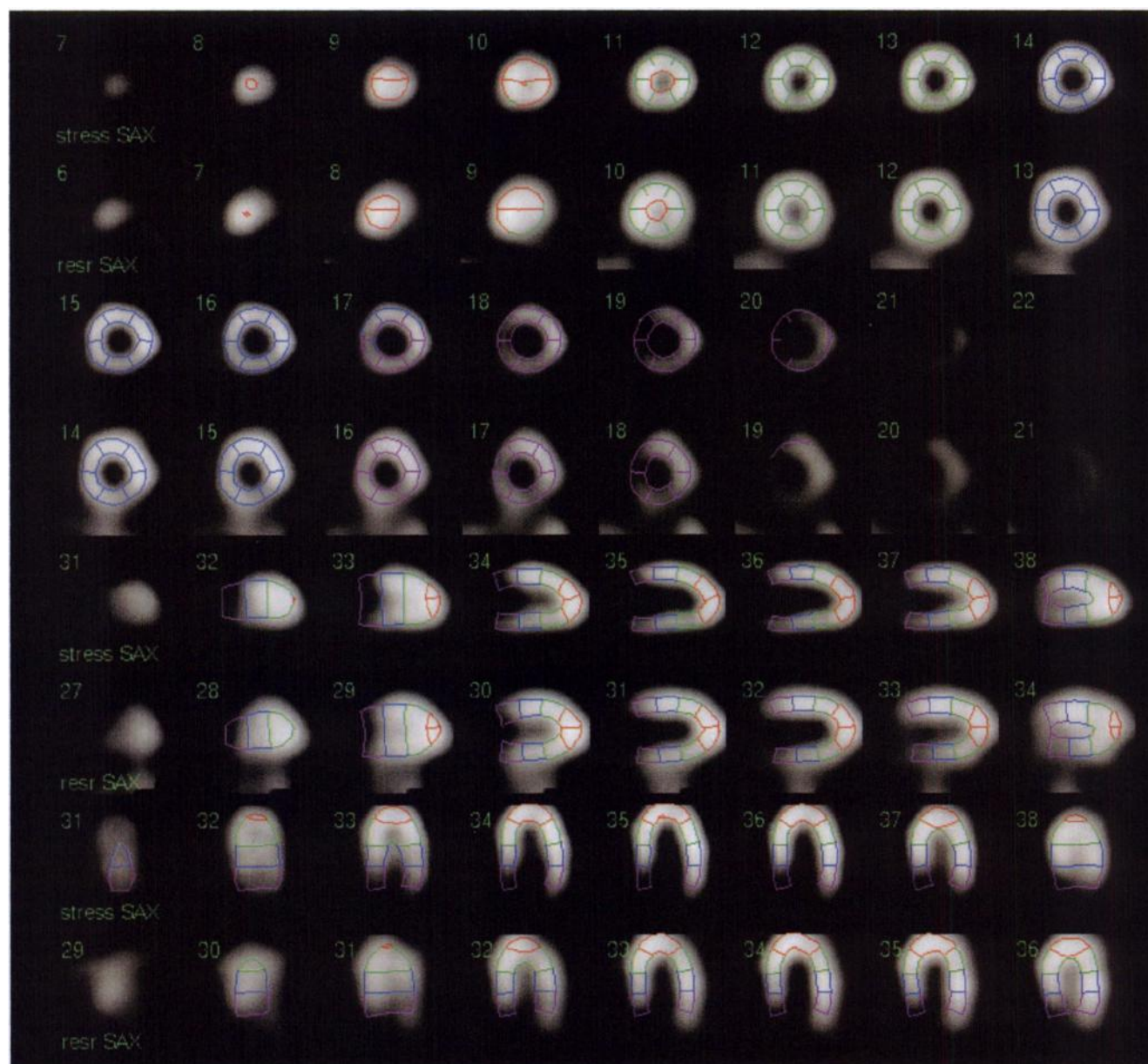

FIGURE 5. Interleaved stress–rest short-axis, vertical, and horizontal long-axis images with color-coded segmental overlays automatically determined by QPS algorithm.
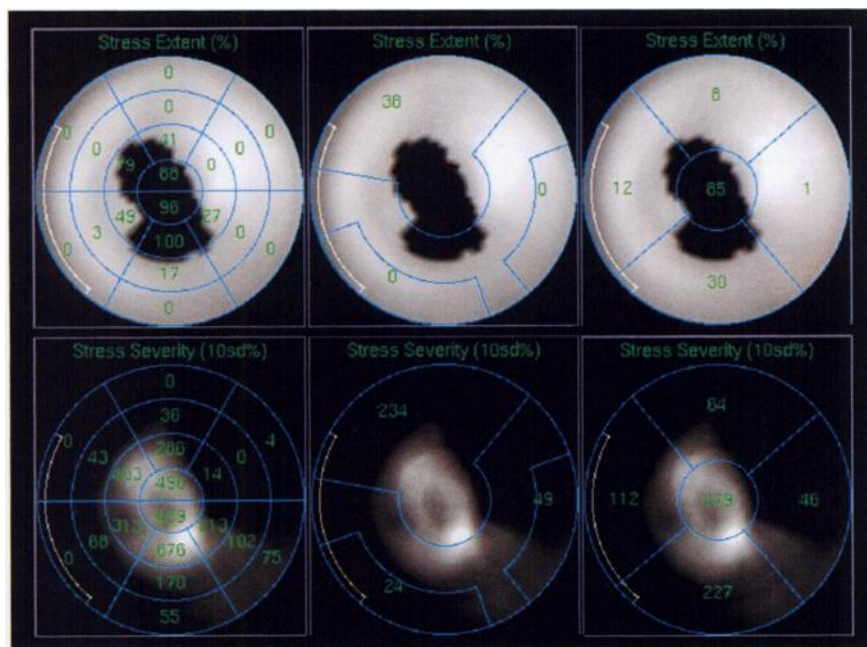
FIGURE 6. Two-dimensional polar maps representing stress defect extent (top row) and severity (bottom row) with 20-segment (left), coronary territory (middle), and myocardial wall (right) overlays for patient in Figures 3–5. Numbers corresponding to regions of overlays express percentage of abnormal myocardial pixels in that region (extent) or degree to which overall region is abnormal (severity).

tional, Inc., Cleveland Heights, OH), or a 1-detector camera (Orbiter; Siemens Medical Systems, Hoffman Estates, IL) and standard acquisition and processing parameters (27).

Inter- and intraobserver reproducibility of the automatic regional and global perfusion scores was tested in 210 patients by applying the algorithm to the data twice and manually constraining the algorithm to operate on a specific portion of the image datasets if it failed to correctly identify the myocardium (27). Assessment of intraobserver reproducibility involved measurements spaced by at least 1 mo.

QPS processing required approximately 5 s on an UltraSPARC1 computer (Sun Microsystems, Inc., Mountain View, CA) with no dedicated or proprietary hardware. The software was modular, was written in the C language, and used an X-Windows graphic user interface and the OSF-Motif toolkit (The Open Group, Menlo Park, CA), making it easily portable within the UNIX environment.

Statistical Analysis

Agreement between successive measurements of global SSS and SRS was assessed using linear regression (Pearson product moment correlation). Agreement between successive measurements of segmental perfusion scores was assessed from 5×5 tables using unweighted κ statistics, with $P < 0.05$ considered statistically significant. Values of $\kappa < 0.4$, between 0.4 and 0.75, and > 0.75 were taken to represent poor, fair to good, and excellent agreement, respectively, on the basis of Fleiss's classification (29). The difference in the success rate of the algorithm between ^{201}Tl studies and ^{99m}Tc-sestamibi studies was evaluated using the χ^2 test.

RESULTS

The algorithm was successful in 397 of 420 patients (94.5%) and 816 of 840 studies (97.1%), with a statistically significant difference between the ^{201}Tl success rate (399/420, or 95.0%) and the ^{99m}Tc success rate (417/420, or 99.3%; $P < 0.001$). Failure was defined as the generation of endocardial and epicardial contours that either did not visually appear to bound the myocardium (10/24, or 41.7%,

9 of which were ^{201}Tl) or overshot the valve plane (14/24, or 58.3%, 12 of which were ^{201}Tl). Failure was invariably caused by the presence of substantial hepatic or intestinal uptake, low myocardial counting statistics, or a combination of these. The user interface of the software allows manual placement of a 3-dimensional ellipsoid region of interest around the myocardium, thus constraining segmentation and surface detection to the portion of the image within the region of interest. This approach was applied to the 24 instances in which the algorithm failed, always resulting in successful completion of processing. The reproducibility of the quantitative results was analyzed because of this limited manual intervention in some of the studies.

Comparisons of the segmental perfusion scores that the algorithm produced automatically when applied by 2 operators (who included manual steps when necessary) to the same 210 patients are shown in Tables 1 and 2 for stress and rest studies, respectively. The exact agreement was 99.9% for both the stress table and the rest table, with a κ of 0.998 for stress and a κ of 0.997 for rest, indicating extremely high reproducibility. The reproducibility of the relative quantita-

TABLE 1
Agreement Table for Stress ^{99m}Tc-Sestamibi Studies

First operator	Second operator				
	0	1	2	3	4
0	2779	1	0	0	0
1	2	647	1	0	0
2	1	0	416	0	0
3	0	0	0	252	0
4	0	0	0	0	101

Table shows agreement in segmental perfusion scores of 2 operators applying QPS to 210 patient studies. $\kappa = 0.998$.

TABLE 2
Agreement Table for Rest ^{201}Tl Studies

First operator	Second operator				
	0	1	2	3	4
0	3704	1	0	0	0
1	1	270	0	0	0
2	0	1	122	0	0
3	0	0	0	59	0
4	0	0	0	0	41

Table shows agreement in segmental perfusion scores of 2 operators applying QPS to 210 patient studies. $\kappa = 0.997$.

tive SSS and SRS measurements was equally high, resulting in regression lines essentially superimposed to the identity line (y = 0.02 + 0.999x, r = 0.999, and SEE = 0.14 for SSS; y = 0.01 + x, r = 1.000, and SEE = 0.07 for SRS; P < 0.001 for both), as shown in Figures 7 and 8. The reproducibility of quantitative measurement of global defect extent (expressed as the global percentage of abnormal myocardial pixels) followed the same pattern (y = -0.05 + 1.001x, r = 0.999, and SEE = 0.17 for stress defect extent; y = 0.997x, r = 1.000, and SEE = 0.09 for rest defect extent).

DISCUSSION

We have described a new automatic method for the quantitation of myocardial perfusion that considers the 3-dimensionality of the left ventricular myocardium. Although the SPECT image volume consists of several stacked 2-dimensional short-axis slices, the QPS algorithm addresses the SPECT image volume 3-dimensionally. From each myocardium, we took a constant number of uniformly distributed samples that were independent of the myocardial size and shape and ensured accurate data registration from different patients. Moreover, sampling followed an ellipsoid model, thus increasing the likelihood that the sampling rays would be perpendicular to the myocardium, and sampling
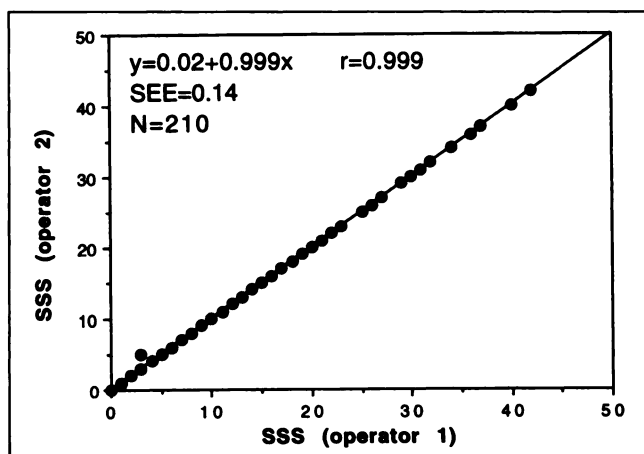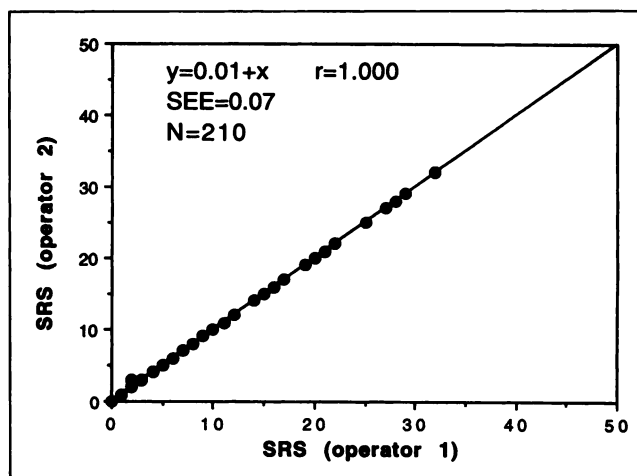
FIGURE 8. Reproducibility of quantitative global SRS scores measured by QPS in 210 patients.

noise was reduced by averaging all data points between the endocardium and the epicardium along each sampling ray (whole-myocardium sampling).

Three-dimensional sampling means that normal limits can be thought of in terms of a fixed number of points corresponding to standard myocardial locations, rather than a variable number of circumferential profiles averaged across patients with potentially wide differences in myocardial size. The myocardium of every patient studied then contributes the same number of data points, which can be compared with the normal myocardial points for the specific protocol used. The dependency of normal limits on the sex of the patient and the radioisotope and protocol used is particularly important today, when wide acceptance of ^{99m}Tc-based agents, different approaches to imaging them, and implementation of manufacturer-specific attenuation correction algorithms have led to proliferation of normal limits far beyond those predicted in the early days of ^{201}Tl quantitation. We have addressed this issue by making generation of normal limits automatic and accessible to the user, who can create and validate limits specific to individual clinical practices and patient populations. However, the future will likely bring a consolidation into classes of normal limits that span protocols and agents.

Three-dimensional sampling and analysis can be carried over to parametric display (Fig. 3), overcoming the geometric distortions introduced by 2-dimensional polar mapping. Three-dimensional displays simplify visual gauging of the extent of a perfusion defect and have been suggested as a way to improve localization of a defect to a specific territory (30), especially in patients with mild or moderate coronary artery disease.

Finally, although the concept of summed perfusion scoring based on a 20-segment, 5-point model has proven extremely important diagnostically and prognostically, scoring remains time consuming and prone to errors and interobserver (as well as intraobserver) variability (25,26). We have addressed this problem by designing the QPS

FIGURE 7. Reproducibility of quantitative global SSS scores measured by QPS in 210 patients.

algorithm to provide a color-coded overlay to facilitate segment identification (Fig. 5) and to automatically generate segmental scores analogous to those used in visual assessment of perfusion. The interpreting physician can opt to modify individual scores to reflect attenuation artifacts and other patient-specific clinical considerations. The CS-20 approach is an accurate, fast, and extremely reproducible way to derive indices of regional and global myocardial perfusion that are directly analogous to those derived by visual inspection and applied to diagnostic and prognostic studies (27).

CONCLUSION

Our automatic approach to the quantitation of myocardial perfusion SPECT incorporates several new techniques based in 3-dimensional space, has an extremely high success rate, and is highly reproducible in a large population of patients. Although we do not recommend that any quantitative algorithm be used indiscriminately and in lieu of expert visual interpretation, we believe that our method represents a useful tool for interpreting physicians in daily clinical practice. We anticipate special value for this software in generation of standardized regional and global perfusion scores and in serial evaluation of patients undergoing medical therapy or revascularization.

ACKNOWLEDGMENT

REFERENCES

1. Maddahi J, Garcia EV, Berman DS, Waxman A, Swan HJ, Forrester J. Improved noninvasive assessment of coronary artery disease by quantitative analysis of regional stress myocardial distribution and washout of thallium-201. Circulation. 1981;64:924–935.
2. Watson DD, Campbell NP, Read EK, Gibson RS, Teates CD, Beller GA. Spatial and temporal quantitation of plane thallium myocardial images. J Nucl Med. 1981;22:577–584.
3. Garcia E, Maddahi J, Berman D, Waxman A. Space/time quantitation of thallium-201 myocardial scintigraphy. J Nucl Med. 1981;22:309–317.
4. Lim YL, Okada RD, Chesler DA, Block PC, Boucher CA, Pohost GM. A new approach to quantitation of exercise thallium-201 scintigraphy before and after an intervention: application to define the impact of coronary angioplasty on regional myocardial perfusion. Am Heart J. 1984;108:917–925.
5. Wackers FJ, Fetterman RC, Mattera JA, Clements JP. Quantitative planar thallium-201 stress scintigraphy: a critical evaluation of the method. Semin Nucl Med. 1985;15:46–66.
6. Van Train KF, Berman DS, Garcia EV, et al. Quantitative analysis of stress thallium-201 myocardial scintigrams: a multicenter trial. J Nucl Med. 1986;27:17–25.
7. Tamaki N, Yonekura Y, Mukai T, et al. Stress thallium-201 transaxial emission computed tomography: quantitative versus qualitative analysis for evaluation of coronary artery disease. J Am Coll Cardiol. 1984;4:1213–1221.
8. Caldwell JH, Williams DL, Harp GD, Stratton JR, Ritchie JL. Quantitation of size of relative myocardial perfusion defect by single-photon emission computed tomography. Circulation. 1984;70:1048–1056.
9. Garcia EV, Van Train K, Maddahi J, et al. Quantification of rotational thallium-201 myocardial tomography. J Nucl Med. 1985;26:17–26.
10. DePasquale EE, Nody AC, DePuey EG, et al. Quantitative rotational thallium-201 tomography for identifying and localizing coronary artery disease. Circulation. 1988;77:316–327.
11. Maddahi J, Van Train K, Prigent F, et al. Quantitative single photon emission computed thallium-201 tomography for detection and localization of coronary artery disease: optimization and prospective validation of a new technique. J Am Coll Cardiol. 1989;14:1689–1699.
12. Klein JL, Garcia EV, DePuey EG, et al. Reversibility bull's-eye: a new polar bull's-eye map to quantify reversibility of stress-induced SPECT thallium-201 myocardial perfusion defects. J Nucl Med. 1990;31:1240–1246.
13. Van Train KF, Areeda J, Garcia EV, et al. Quantitative same-day rest-stress technetium-99m-sestamibi SPECT: definition and validation of stress normal limits and criteria for abnormality. J Nucl Med. 1993;34:1494–1502.
14. Van Train KF, Garcia EV, Maddahi J, et al. Multicenter trial validation for quantitative analysis of same-day rest-stress technetium-99m-sestamibi myocardial tomograms. J Nucl Med. 1994;35:609–618.
15. Benoit T, Vivegnis D, Foulon J, Rigo P. Quantitative evaluation of myocardial single-photon emission tomographic imaging: application to the measurement of perfusion defect size and severity. Eur J Nucl Med. 1996;23:1603–1612.
16. Garcia EV, Cooke CD, Van Train KF, et al. Technical aspects of myocardial SPECT imaging with technetium-99m sestamibi. Am J Cardiol. 1990;66:23E–31E.
17. Germano G, Van Train K, Kiat H, Berman D. Digital techniques for the acquisition, processing, and analysis of nuclear cardiology images. In: Sandler MP, ed. Diagnostic Nuclear Medicine. Baltimore: Williams & Wilkins; 1995:347–386.
18. Rozanski A, Diamond GA, Forrester JS, Berman DS, Morris D, Swan HJ. Alternative referent standards for cardiac normality: implications for diagnostic testing. Ann Intern Med. 1984;101:164–171.
19. Goris ML, Thompson C, Malone LJ, Franken PR. Modelling the integration of myocardial regional perfusion and function. Nucl Med Commun. 1994;15:9–20.
20. Faber TL, Stokely EM, Peshock RM, Corbett JR. A model-based four-dimensional left ventricular surface detector. IEEE Trans Med Imaging. 1991;10:321–329.
21. Germano G, Kiat H, Kavanagh PB, et al. Automatic quantification of ejection fraction from gated myocardial perfusion SPECT. J Nucl Med. 1995;36:2138–2147.
22. Germano G, Erel J, Lewin H, Kavanagh PB, Berman DS. Automatic quantitation of regional myocardial wall motion and thickening from gated technetium-99m sestamibi myocardial perfusion single-photon emission computed tomography. J Am Coll Cardiol. 1997;30:1360–1367.
23. Germano G, Kavanagh PB, Berman DS. An automatic approach to the analysis, quantitation and review of perfusion and function from myocardial perfusion SPECT images. Int J Card Imaging. 1997;13:337–346.
24. Germano G, Kavanagh PB, Su HT, et al. Automatic reorientation of three-dimensional, transaxial myocardial perfusion SPECT images. J Nucl Med. 1995;36:1107–1114.
25. Berman DS, Hachamovitch R, Kiat H, et al. Incremental value of prognostic testing in patients with known or suspected ischemic heart disease: a basis for optimal utilization of exercise technetium-99m sestamibi myocardial perfusion single-photon emission computed tomography. J Am Coll Cardiol. 1995;26:639–647.
26. Hachamovitch R, Berman DS, Kiat H, et al. Effective risk stratification using exercise myocardial perfusion SPECT in women: gender-related differences in prognostic nuclear testing. J Am Coll Cardiol. 1996;28:34–44.
27. Sharir T, Germano G, Waechter PB, et al. A new algorithm for the quantitation of myocardial perfusion SPECT. II: validation and diagnostic yield. J Nucl Med. 2000;41:720–727.
28. Berman DS, Kiat H, Friedman JD, et al. Separate acquisition rest thallium-201/stress technetium-99m sestamibi dual-isotope myocardial perfusion single-photon emission computed tomography: a clinical validation study. J Am Coll Cardiol. 1993;22:1455–1464.
29. Fleiss JL. Statistical Methods for Rates and Proportions. New York, NY: Wiley; 1973.
30. Cooke CD, Vansant JP, Krawczynska EG, Faber TL, Garcia EV. Clinical validation of three-dimensional color-modulated displays of myocardial perfusion. J Nucl Cardiol. 1997;4:108–116.